Louis, L., Day-Stirrat, R., Hofmann, R., Saxena, N., Schleicher, A. M. (2018): Computation of effective elastic properties of clay from X-ray texture goniometry (XTG) data. - *Geophysics*, *83*, 5, pp. MR245—MR261.

DOI: http://doi.org/10.1190/geo2017-0581.1

GEOPHYSICS, VOL. 83, NO. 5 (SEPTEMBER-OCTOBER 2018); P. MR245–MR261, 17 FIGS., 2 TABLES.
10.1190/GEO2017-0581.1

Computation of effective elastic properties of clay from X-ray texture goniometry data

Laurent Louis[1], Ruarri Day-Stirrat[2], Ronny Hofmann[2], Nishank Saxena[2], and Anja M. Schleicher[3]

ABSTRACT

We have developed a new method for estimating the contribution of a pure clay fraction (i.e., devoid of organic matter) to the total effective rock stiffness. The method is based on published clay mineral stiffness data and on an original preferred clay mineral orientation data set obtained by X-ray texture goniometry on 56 samples of Kimmeridgian and Devonian age from two North American shale plays. We find that (1) large variability in preferred orientation of clay results in moderate variability in effective clay elastic anisotropy and (2) the effect of variations in the preferred orientation on effective rock properties is small compared with the effects of variations in clay abundance. As a result, a single clay elastic tensor is computed to be used in effective medium models. In addition, to account for various degrees of hydration, water is incorporated into the dry clay tensor through inclusion models. In situations in which isotropic approximations are necessary, we also provide apparent bulk and shear moduli for a hydrated clay fraction as a function of porosity and propagation angle.

INTRODUCTION

Clay mineral volume and alignment significantly impact many properties of resource shale plays, including porosity, fluid saturation, resistivity, stiffness, and strength. In the case of elasticity, the anisotropy resulting from preferential orientation of clay particles causes considerable uncertainty in petrophysical modeling. Taken alone, an individual clay particle can exhibit intrinsic anisotropy leading to variations in moduli between 50% and 300%. Therefore, forward modeling of the contribution of clay to rock elastic properties should include a dependency on the propagation angle with respect to the anisotropy directions.

The literature is rich with studies that include the preferred orientation in relation to consolidation (Curtis et al., 1980; Day-Stirrat et al., 2010a), smectite-to-illite transformation (Ho et al., 1999; Day-Stirrat et al., 2008), low-grade metamorphism (Ho et al., 1995; Jacob et al., 2000), or even faulting (Solum et al., 2003, 2005; Haines et al., 2009; Solum and van der Pluijm, 2009). In the realm of shale rock petrophysics, acoustic anisotropy is a long-recognized characteristic, which still presents modeling (hence, inversion) challenges in terms of individual constituents properties and in terms of effective medium representation (e.g., Rundle and Schuler, 1981; Banik, 1984; Hornby et al., 1994; Sayers, 1994, 1999, 2005, 2008, 2013; Johnston and Christensen, 1995; Vernik and Landis, 1996; Vernik and Liu, 1997; Hornby, 1998; Cholach and Schmitt, 2006; Moyano et al., 2012; Vasin et al., 2013; Allan et al., 2015). Further studies investigating the relationship between fabric and effective properties are still required. Such studies can provide building blocks conducive to better estimates of critical quantities such as porosity, hydrocarbon saturation, and geomechanical properties.

This work consists of two parts. In the first part, a method for analyzing the raw X-ray texture goniometry (XTG) preferred orientation data is defined. In the second part, an effective clay tensor for the clay fraction is calculated in two suites of shale samples of Kimmeridgian and Devonian age based on XTG data to provide reference values for rock-modeling applications.

Among various techniques available to characterize and quantify the preferred orientation of clay minerals, X-ray diffraction using texture goniometry in transmission mode (XTG) has been historically widely used (Sintubin, 1994; van der Pluijm et al., 1994). The XTG technique is statistically representative and repeatable, and it offers a large output data set in a reasonable timeframe. In total, 39 samples of

Manuscript received by the Editor 30 August 2017; revised manuscript received 4 April 2018; published ahead of production 22 May 2018; published online 18 July 2018.
[1]Formerly Shell International Exploration and Production, Houston, Texas, USA; presently New England Research, White River Junction, Vermont, USA. E-mail: llouis@ner.com.
[2]Shell International Exploration and Production, Houston, Texas, USA. E-mail: ruarri.day-stirrat@shell.com; ronny.hofmann@shell.com; nishank.saxena@shell.com.
[3]GFZ German Research Centre for Geosciences, Helmholtz Center Potsdam, Potsdam, Germany. E-mail: aschleic@gfz-potsdam.de.

Kimmeridgian age and 17 of Devonian age from two North American shale plays were measured using that technique at the University of Michigan (UM) for chlorite and illite basal spacings. The data were then reprocessed as a mean to compare alternate ways of quantifying preferred orientation and allow further exploitation. As a result, a method that leads to the smallest residuals is picked.

In the second part of this study, the results from the orientation data analysis are used as input in a code that calculates the effective properties of a dry clay aggregate for each sample and the associated illite/chlorite ratio (obtained from XRD), based on published elastic properties for single crystals. The elastic anisotropy associated with the orientation data is then analyzed for P- and S-wave moduli. We also calculate isotropic moduli for a "randomly" oriented set of particles to compare with published data and with what is later referred to as "apparent" or "pseudo" isotropic moduli.

The comparison between XTG data and calculated elastic tensors shows that a wide range of preferred orientation intensities results in moderate elastic anisotropy. Moreover, a calculation comparing the respective effects of changes in preferred orientation and clay content on effective solid fraction properties shows that the effect of clay content is clearly dominant. Therefore, we conclude that the use of a single average clay tensor in the Kimmeridgian and Devonian Shale rocks studied is a sufficient approximation. This also offers great simplification for modeling because a unique set of effective clay properties can be used as is already the case for quartz, calcite, feldspar, and other common minerals. To facilitate the use of this result in quantitative interpretation applications, we perform two additional tasks. First, apparent isotropic elastic moduli are calculated as a function of dip angle for our results to also be used in isotropic elastic models. Second, we also compute results for a clay fraction containing varying amounts of water using inclusion models. This is done using first a straightforward approach (the average of the Hashin-Shtrikman bounds), and then we use an elaborate one (implementation of the effect of saturated ellipsoidal cavities on anisotropic background proposed by Sevostianov et al., 2005). Using the latter approach, substantial anisotropy is preserved even for high-water-fraction (or "porosity") values, suggesting that in vertical transverse isotropic (VTI) media, the angle between the symmetry axis and propagation direction should be used to account for the effect of the anisotropic clay component.

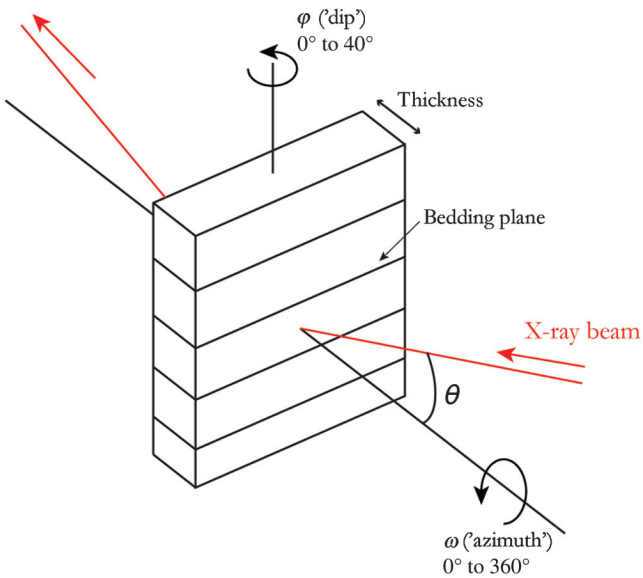

Figure 1. Example of a sample setup. The diffraction angle θ corresponding to the phase of interest is set and maintained constant throughout the rotation. An intensity measurement is carried out for all (ω, φ) combinations with ω varying from 0° to 360° by increments of 2.5°, and φ varying from 0° to 40° by increments of 5°.

REDUCTION OF XTG DATA

High-resolution XTG

The following overview describes the system in use at the Department of Geological Sciences at UM. All XTG data used in this paper were obtained at that facility. Quantitative assessment of the alignment of clay minerals is made on an Enraf-Nonius CAD4 automated single-crystal diffractometer using the high-resolution XTG (HRXTG) method described by van der Pluijm et al. (1994). HRXTG analysis is a two-step process. First, the samples are scanned over the range of 0.5°2θ–6.0°2θ MoKα (1°2θ–13°2θ in CuKα for reference). This indicates which clay mineral phases are present and determines the exact diffraction angles at which textural data should be collected. The second step of the measurement process involves the "pole-figure scan" (Ho et al., 1995), in which the degree of preferred orientation of previously identified clay minerals is determined. In this step, the goniometer and detector were fixed at the diffraction angle corresponding to the d-spacing of the 00l reflection of the chosen phase as defined in the so-called 2θ scan. Samples are then rotated around two axes, one parallel to an imaginary line connecting the goniometer and detector (around which the angle ω is measured) and one normal to it (around which φ is measured). Figure 1 provides a generic setup with the X-ray beam and diffraction angle fixed (in red), and the two rotation angles ϕ and ω. Diffracted X-ray intensity data are collected every 2.5° between 0° and 360° around the "ω-axis," and in nine steps between 0° and 40° around the "φ-axis." In total, 1296 intensity measurements are thus made on each sample.

Samples are prepared using the glass slide transfer method in which a face is cut and ground flat and then adhered to a glass slide. The other side of the parallel face is cut using a slow-speed diamond-tipped saw blade. This face is then ground further to achieve as thin a slab as possible for transmission work. The ideal sample thickness is 100 μm, but in practice some samples are slightly thicker. Exact thicknesses are individually measured with a caliper then used in the data-analysis process.

A typical result for a 0.5°2θ–6.0°2θ MoKα scan is shown in Figure 2a with the illite and chlorite peaks marked. Figure 2b and 2c shows the corresponding pole figures obtained for illite and chlorite, respectively. The degree of alignment is obtained from the intensity distribution of diffracted X-rays. Intensity data are displayed in pole figure diagrams that show the distribution of crystallographic orientations in the form of poles to crystallographic planes. Pole figure diagrams visualize the spatial distribution of the X-ray intensities by displaying contour lines representing the pole distribution of clay minerals (001) plane orientations. The degree of particle alignment is expressed as maximum pole density in multiples of a random distribution (MRD) (Wenk, 1985), where greater values reflect greater degrees of alignment. Intensity depends on the concentration of crystals aligned parallel to each other. A value for the MRD is produced even when the sample has not been prepared perpendicular to bedding, so a lower hemisphere equal area projection showing centered contour

lines validates the MRD value. The final values are normalized to be free of sample parameters such as mineral content by summing all the data points over the whole pole figure and weighing them with respect to their areal distribution (van der Pluijm et al., 1994).

Matrix characterization by X-ray diffraction

To progress the analysis and exploitation of orientation data, the relative abundance of each analyzed clay type must be known. Mineralogical data are used in several ways: first to probe the link between clay abundance and preferred orientation and then to compute the actual effective elastic tensor. Ultimately, bulk mineralogical characterization can be used for complete modeling of the elastic properties of the solid fraction.

Preparation, machine settings, and pattern interpretation used the same methods as presented in Day-Stirrat et al. (2010b). Random powders of bulk samples were prepared using a spray-drying technique in which slurry material, ground to 10 μm using a micronizing mill in an ethanol medium, was passed through a warm column of air (60°C). The initial qualitative phase identification occurs manually. A library of geologic standards was selected for quantification using a simple solver method. Patterns on all library standards were previously acquired on the same machine under the same settings. The library standard of a particular mineral was analyzed with 20% corundum. No internal standard was used for the experiment, but analysis of the produced patterns was carried out using a normalized full pattern reference intensity ratio method based on mineral standards, in which an internal standard was used. Expanded uncertainty using a coverage factor of two, i.e., 95% confidence, is given by $\pm X^{0.35}$, where X is the concentration in wt%, e.g., 30 wt% ±3.3. X-ray powder diffraction patterns were recorded from 2°2θ to 75°2θ using cobalt Kα radiation.

Because the calculations performed in this work require the use of volumetric fractions as opposed to weight fractions, weights were converted into volumes using the following equation:

$$v_i = \frac{w_i/\rho_i}{\sum_{k=1}^{n} w_k/\rho_k}, \tag{1}$$

where v represents the volume fraction, w is the weight fraction, and n is the number of phases.

Orientation data analysis workflow

The orientation analysis workflow detailed here was developed and globally follows the protocol summarized above, albeit with two main differences being the use of (1) a geometric correction for the position of the pole to bedding and (2) a phenomenological fitting function obtained from March's (1932) theory (Owens, 1973; Oertel, 1983).

Background, absorption, and irradiation corrections

The background correction is based on a 2θ scan that provides an empirical relationship between the background X-ray intensity and the 2θ angle. This background effect equates to approximately 20 counts at a d-spacing of 10 Å (mica) and approximately 14 counts at 7 Å (chlorite). When tilting a sample away from perpendicular to the incident X-ray beam, the path length and the irradiated volumes increase. Increase of the path length results in higher X-ray absorption, hence a lower measured X-ray intensity. On the other hand, an increase of the irradiated volume results in an increase of the X-ray diffraction path length because more material is being probed. The total change in X-ray intensity is therefore a function of both effects. To be calculated, those effects require the input of a mass absorption coefficient, a density, and a sample thickness. Although the sample thickness varies from sample to sample, the mass absorption coefficient and the density of quartz are used throughout (respectively 3.66 cm^2/g and 2.65 g/cm^3).

The expression used for calculating the corrected intensity is

$$I_{\alpha,\mathrm{cor}} = \frac{(I_{\alpha,\mathrm{meas}} - I_{\mathrm{background}})}{\delta_a(\alpha) \times \delta_i(\alpha)}, \tag{2}$$

where α is the tilt angle and δ_a and δ_i are the absorption and irradiation correction factors, respectively.

Once the intensities have been corrected, these values need to be normalized so the preferential orientation can be expressed in units of the so-called MRD. Normalization is done by averaging over all orientations the intensities weighed with respect to their areal contribution in the pole figure:

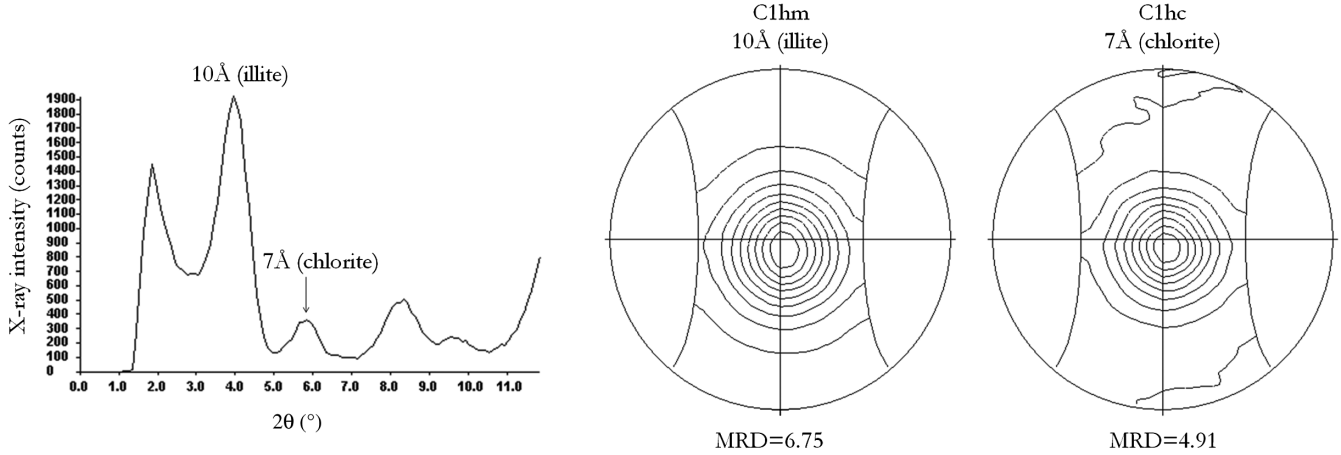

Figure 2. Typical output provided by UM for a given sample. (a) Result of a 0.5°2θ–6.0°2θ MoKα scan with the illite and chlorite peaks marked. (b) Pole figure for illite with MRD. (c) Pole figure for chlorite with MRD.

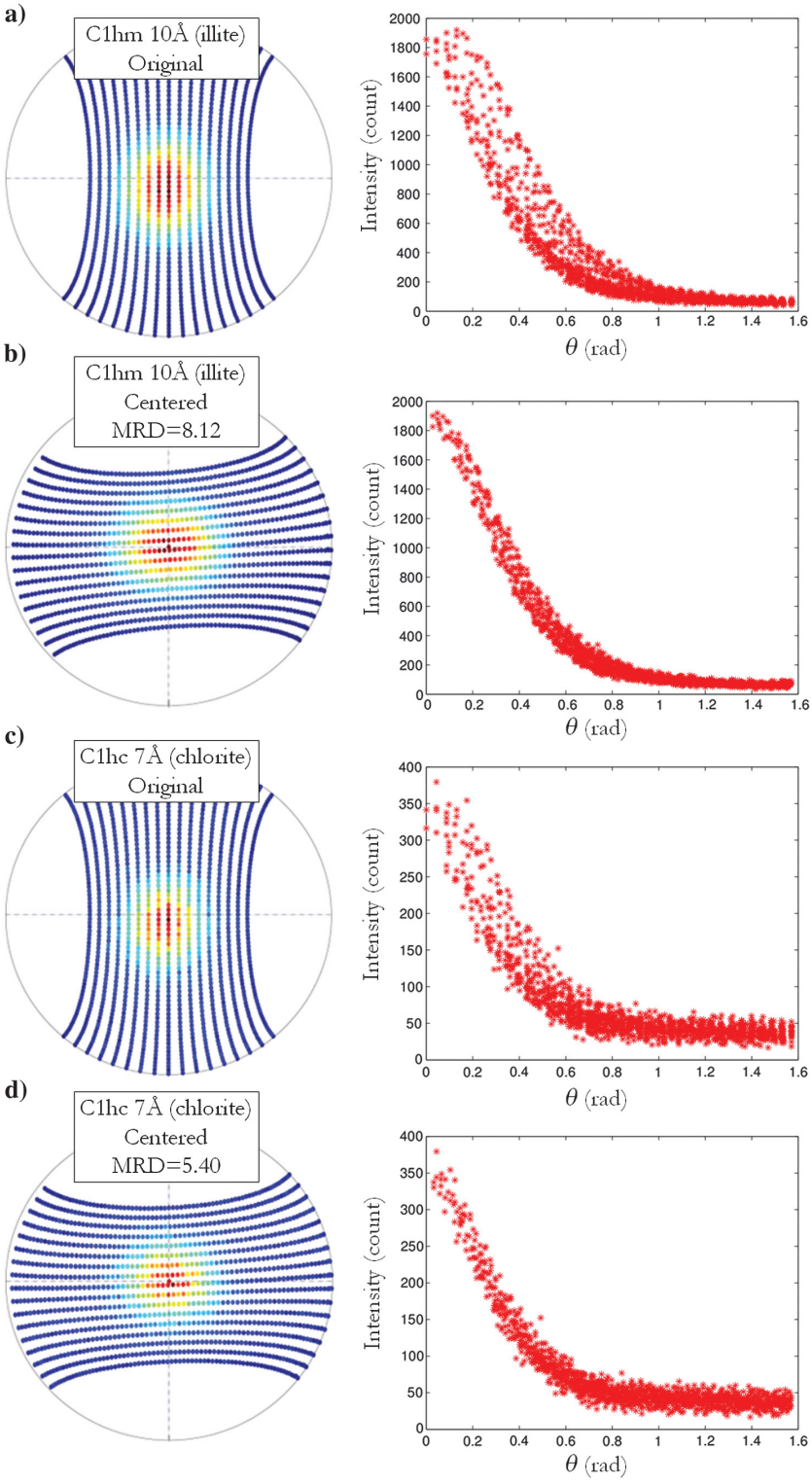

Figure 3. Effect of centering the data set on the circumferential collapse for the same sample as in Figure 2. (a) Illite raw data, (b) illite rotated data, (c) chlorite raw data, and (d) chlorite rotated data. Note the substantial reduction in scatter on the circumferentially collapsed profiles after centering.

$$I_\alpha^{\text{norm}} = I_\alpha \times \frac{\sum_\alpha \sin(\alpha)}{\sum_\alpha I_\alpha \times \sin(\alpha)}. \qquad (3)$$

In the above normalization, I_α represents the average intensity measured at the tilt angle α.

Centering and circumferential collapse

As can be seen on the illite and chlorite pole figures in Figure 2b and 2c, the center of the distributions does not coincide perfectly with the center of the projection due to the inherent misalignment between the initial sample position and the pole to bedding. The magnitude of this misalignment varies from sample to sample, but it is unavoidable because (1) the bedding plane must be clearly visible and (2) the accuracy of the positioning perpendicular or parallel to the holder axis is manually controlled by the operator. The effect of this misalignment is illustrated in Figure 3a and 3c for the illite and chlorite peaks, respectively. The data set is the same as the one in Figure 2, but it is reprocessed. In both cases, a circumferential collapse of the data onto an intensity versus tilt plot shows a scatter that results from that misorientation. To correct for this effect and improve the accuracy of the MRD estimate, a rotation of the data set in the reference formed by the eigenvectors is done prior to the circumferential collapse. The result can be seen for both peaks in Figure 3b and 3d, where the scatter is virtually suppressed. The MRD values compare clearly higher than the UM example, although this difference is essentially due to the approach taken with the fitting function (see the next section). In the present case, the centering represents in fact a minor change but it allows the workflow to handle strong misorientations while taking advantage of all the data at hand through the circumferential collapse. The azimuthal rotation of almost 90° that is observed has no incidence on the final distribution. This rotation is controlled by the calculation of the eigenvectors, whereby the major principal axis is directed outward from the plane of the figure and the minor one is pointing up in the plane of the figure (the intermediate being horizontal pointing to the right).

Note that the clay fabric is assumed here to have a VTI symmetry, although slight anisotropy is present within the plane of the figure in the pole diagrams. This anisotropy is responsible for some of the remaining scatter and represents approximately a 100th of the one measured between the bedding plane and its pole. Such anisotropy is in essence neglected in the circumferential collapse, but it is possible that careful study of this component would yield some insight of tectonic nature provided that samples have been geographically reoriented beforehand.

Fitting a distribution

The second step of the data-reduction workflow is the fitting of the circumferentially collapsed distributions. Several solutions can be used to describe preferential orientation away from the symmetry axis (Baker et al., 1993; Johansen et al., 2004). Three were found to provide reasonable fits to the data: a simple exponential fit; the Bingham distribution; and the Owens-March distribution, which is based on grain-rotation kinematics. The equations are as follows:

$$\text{Exponential(two-fitting parameters)}\ f(\alpha) = f(0) \times e^{-c\alpha}, \tag{4}$$

$$\text{Bingham(two-fitting parameters)}\ f(\alpha) = f(0) \times e^{-d.\cos^2(\alpha)}, \tag{5}$$

$$\text{Owens-March(one-fitting parameter)} f(\alpha) = \frac{Z}{[Z^2 + \sin^2(\alpha) * (1 - Z^2)]^{3/2}}, \tag{6}$$

where α is the inclination angle away from the vertical axis and c, d, and Z are fitting parameters. Parameter Z in the Owens-March approach carries some additional meaning in that it is associated to the strain applied to an initially randomly oriented set of lines (March, 1932; Owens, 1973; Oertel, 1983). The March model indeed considers a set of imaginary lines or planes that get progressively reoriented in response to the application of a strain tensor. This model has been largely used in studies relating fabrics and tectonic deformation (Curtis et al., 1980; Oertel, 1983; Evans et al., 1989; Henry et al., 2003). The expression in equation 6 corresponds to a uniaxial strain case and the parameter Z stands for the macroscopic strain defined as $Z = l_{\text{final}}/l_{\text{init}} = (1 - e_v)$, where l_{final} and l_{init} would be the initial and final lengths of the aggregate of planar objects being shortened and e_v is the incremental strain defined as $e_v = dl/l$.

Figure 4a shows the same data as Figure 3b, and the best fit is shown in Figure 4b for the three functions considered after the data have been normalized according to equation 3. The parameters for the best fit are calculated using the least-squares method for the exponential and Bingham functions and retrieved by iteration for the Owens-March model. Before these best fits are obtained, the distributions are rebinned so as to not over-represent the intensities at a high angle, which are numerous compared with low-angle ones but also represent a small portion of the surface in the normalized distribution. Bins were made equally distant on a logarithmic scale as would be done for fitting a normal distribution, to approach a constant number of data points per bin. The result of this rebinning is shown in Figure 4b and represents the data to be fitted. For the case selected, the fit appears much better for the Owens-March function in comparison with the exponential and Bingham ones, which respectively over- and underestimate the MRD values. To further assess the quality of the fits, a residual was calculated for an entire data set, as shown in Figure 5. The expression used for the residual is

$$r = \frac{\sum_\alpha (I_{\text{fit}} - I_{\text{meas}})}{\sum_\alpha (I_{\text{meas}})}. \tag{7}$$

Although it uses only one fitting parameter, in most cases, the Owens-March approach is the one that fits best the orientation data. In addition to its simplicity, the Owens-March approach is tied to a model of grain reorientation as a function of uniaxial strain. Indeed, using equation 6 with the definition of Z, one can write

$$\text{MRD} = f(0) = \frac{1}{Z^2} = \frac{1}{(1 - e_v)^2}. \tag{8}$$

Hence directly relating the incremental strain with MRD.

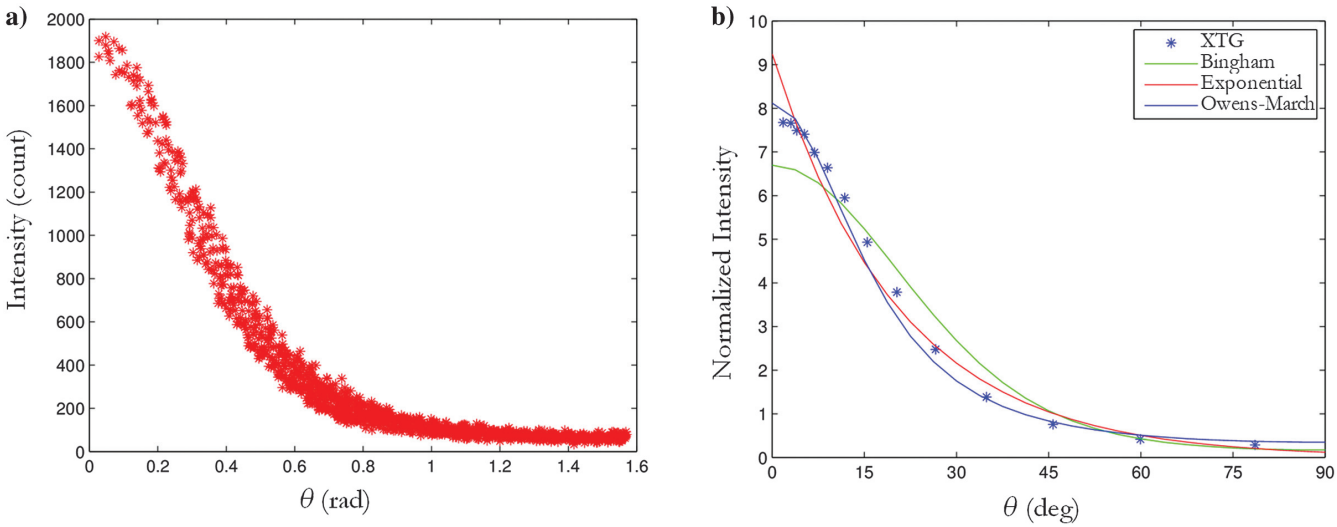

Figure 4. Comparison between three candidate fitting functions for the illite orientation data on sample KS-C1H, after normalization according to equation 3.

Results

This analysis was conducted on 56 samples from two shale plays in the continental United States (southern and northeastern). Here, 39 of them are of Kimmeridgian (Upper Jurassic) age and 17 of Devonian age, and all have undergone significant diagenesis. The samples come from wells with thermal maturities greater than 1.4% vitrinite reflectance, placing them in the dry gas window. The sampled sections are over a narrow depth interval (<50 m), and we assume, therefore, that diagenetic and thermal histories are similar between samples from the same well. Clay types are very similar from their diffraction patterns but vary in abundance. In situ total organic carbons range from 0.5 wt% to 5 wt%, and based on the maturity and maceral types present, most of the organic matter no longer resides in a depositional location.

Tables 1 and 2 provide XRD and HRXTG data obtained in the two formations, respectively. Globally, the mineralogy is dominated by clay, with a relatively constant quartz component (approximately 25%) and a highly variable carbonate fraction (approximately 10%–50%), which correlates negatively with the clay abundance. Feldspars represent a stable contribution at approximately 5%–10%. In Figure 6, the preferred orientation results are analyzed and compared with clay abundance. Figure 6a and 6b shows (1) a more than two MRD unit difference between illite and chlorite and (2) a strong control of the MRD values by the clay content. The relationship that is observed appears to encompass very well the results reported for other shales (e.g., Wenk et al., 2008; Kanitpanyacharoen et al., 2012). The difference between illite and chlorite is thought to be controlled by the effect of crystallite size/shape on the reorientation process during compaction and to other diagenetic processes. If each clay mineral is considered individually, however, the overlay between the data sets from the two formations is very good. This suggests, at least for illite, a robust transform between clay content and preferred orientation in shales (approximated with the linear best fits in Figure 6a). Note that the plots implicitly assume that the trends are independent of the actual relative abundances of illite and chlorite. According to the XRD data, illite is in fact consistently present in a much larger amount relative to chlorite.

In studies relating clay fabrics to deformation, an apparent requirement for strong preferred orientation is the presence of higher amounts of clay within the solid fraction (Curtis et al., 1980; Day-Stirrat et al., 2010a). As the clay fraction decreases, the likelihood of relatively rounder grains achieving continuous contact throughout the aggregate increases, what in effect prevents further reorientation of the platy particles. Therefore, the "strain" recorded by the preferred orientation is also (and may be primarily) a measure of the clay content.

Because the Owens-March model is used, the equivalent uniaxial strain can be calculated from MRD as given in equation 8. This is shown in Figure 6c and 6d. The correlation for illite in particular is very good. It is worth noting that for illite, which largely dominates the clay fraction, the equivalent strain for an initially randomly oriented aggregate comprises between 50% and 70%, which is a relatively narrow range.

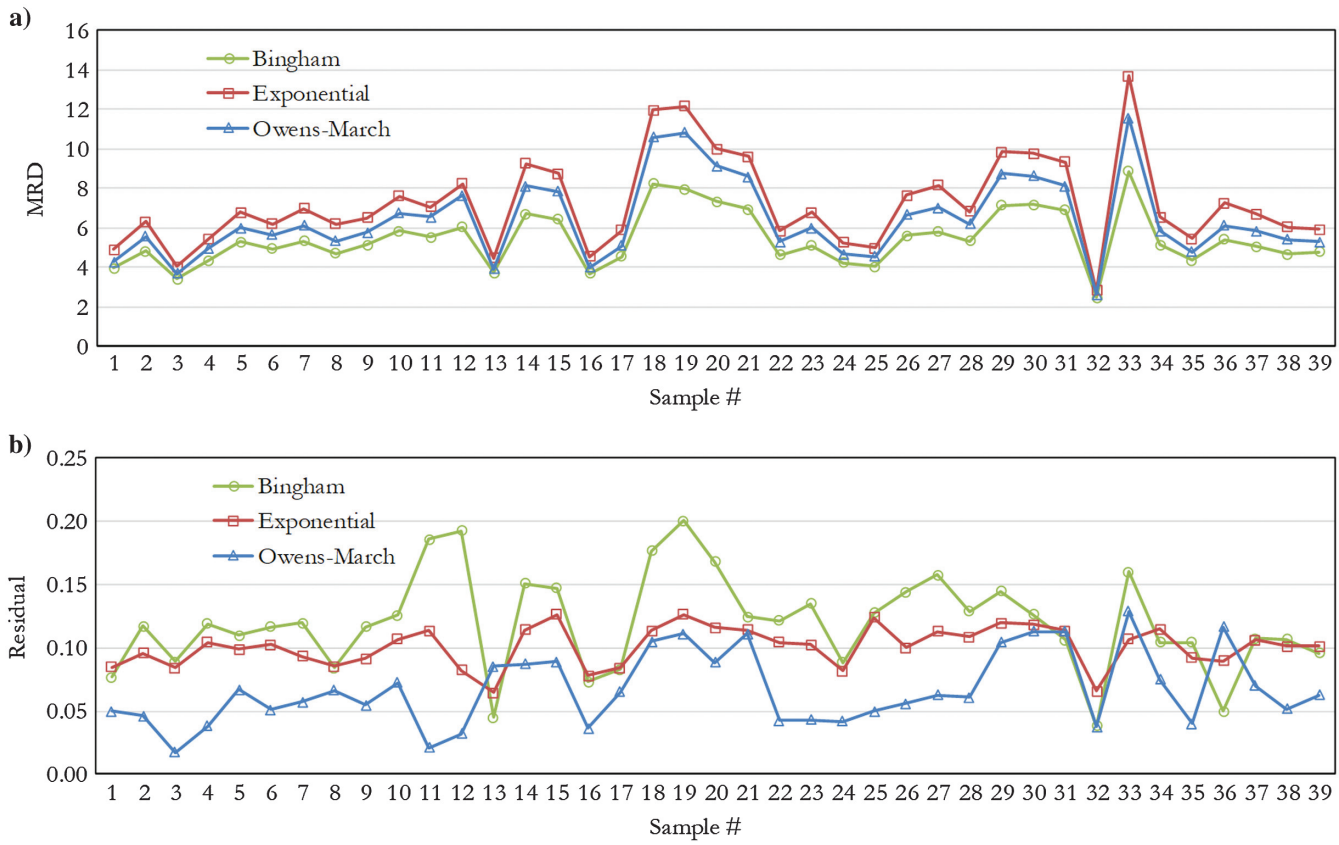

Figure 5. Comparison of the MRD and residuals obtained with the three candidate fitting functions for the illite orientation data on one of our data sets, after normalization according to equation 3.

In summary, a data-reduction workflow for XTG measurements was established that suggests using the Owens-March approach because it produces the smallest residuals after fitting. This model is tied to an apparent uniaxial vertical strain that may be used for interpretation in terms of deformation history. In the following section, effective elastic properties are calculated for the orientation data compiled here.

Table 1. XTG and XRD data for all Kimmeridgian Shale samples studied. KS is used for Kimmeridgian Shale in the sample ID, and the letter refers to the well (five different wells). MRD values from UM and modified workflows are shown for comparison. XRD results are provided in vol% using equation 1.

	MRD illite (UM)	MRD illite (Shell)	MRD chlorite (UM)	MRD chlorite (Shell)	Quartz	K-feldspar	Plagioclase	Calcite	Dolomite	Pyrite	Illite	Di-oct 2:1 clays	Chlorite
ID	XTG				XRD % solid volume								
KS_A1H	3.97	4.27	2.52	2.28	22.70	1.29	6.00	27.74	10.22	1.22	24.20	3.95	2.68
KS_A2H	4.86	5.59	2.93	2.85	27.32	1.51	6.31	23.72	3.50	1.44	26.11	7.90	2.19
KS_A3H	3.47	3.71	—	—	—	—	—	—	—	—	—	—	—
KS_A4H	4.26	4.99	—	—	—	—	—	—	—	—	—	—	—
KS_A5H	5.26	6.01	3.45	3.51	30.23	1.19	7.50	13.90	1.08	1.95	32.07	10.39	1.70
KS_A6H	5.06	5.64	3.43	3.37	25.93	1.61	6.31	23.60	2.04	1.33	26.48	9.61	3.08
KS_A7H	5.2	6.12	3.19	3.20	25.36	1.18	5.49	20.96	3.31	1.72	26.92	11.96	3.09
KS_B1H	4.3	5.36	3.18	3.23	23.17	0.97	11.44	21.82	1.02	1.39	27.85	8.91	3.43
KS_B8H	5.02	5.78	3.74	3.89	23.44	0.97	13.05	21.36	0.49	1.44	29.59	5.98	3.68
KS_B9H	5.8	6.74	4.01	4.46	22.90	0.97	9.83	22.27	1.56	1.33	26.11	11.84	3.18
KS_B7H	5.61	6.56	3.73	3.43	19.61	1.40	16.00	14.38	1.07	1.11	35.36	4.57	6.49
KS_B6H	5.9	7.65	3.7	3.62	23.48	0.54	8.44	9.65	0.49	0.89	42.34	8.36	5.81
KS_B5H	2.91	3.93	2.56	2.50	—	—	—	—	—	—	—	—	—
KS_C1H	6.75	8.12	4.91	5.40	18.93	1.41	4.82	10.65	2.27	1.46	40.43	16.50	3.52
KS_C2H	6.77	7.85	4.81	5.00	18.81	0.86	6.52	23.51	1.27	0.78	32.64	11.14	4.47
KS_C3H	3.72	4.01	2.33	2.23	9.38	2.18	5.36	17.89	37.93	1.29	18.70	0.00	7.26
KS_C5H	4.17	5.09	2.54	2.35	18.24	1.19	9.97	27.53	0.78	1.61	29.48	6.40	4.79
KS_C6H	7.96	10.57	5.82	6.79	21.34	0.65	5.52	9.23	1.96	0.78	38.62	16.60	5.30
KS_C7H	7.95	10.81	5.98	7.06	24.36	3.47	7.82	9.98	2.26	1.06	41.13	0.00	9.92
KS_C8H	7.27	9.15	5.84	6.38	21.30	0.98	6.68	6.35	2.46	0.78	42.52	10.21	8.73
KS_C9H	6.27	8.59	5.35	6.46	21.59	2.04	6.92	22.94	6.80	0.61	29.59	0.00	9.52
KS_D1H	4.58	5.29	3.10	3.01	24.15	0.97	7.69	21.95	15.44	1.39	23.42	0.00	4.99
KS_D2H	5.03	6.01	3.26	3.40	23.57	1.18	6.71	28.38	0.87	1.27	23.64	11.21	3.17
KS_D3H	3.90	4.68	2.49	2.59	22.66	0.85	5.94	43.36	0.77	1.10	20.04	3.11	2.16
KS_D5H	4.42	4.57	2.57	1.82	28.00	1.29	7.47	28.10	0.59	2.16	26.45	4.06	1.89
KS_D6H	5.41	6.66	3.56	3.60	25.16	0.98	6.38	24.69	2.26	2.63	26.09	8.90	2.91
KS_D7H	5.91	7.01	3.85	3.89	27.44	0.43	6.42	21.05	1.95	1.22	29.30	8.71	3.48
KS_D8H	5.32	6.19	3.10	3.06	28.83	1.18	6.59	27.27	0.29	1.32	25.10	7.25	2.17
KS_E1H	6.94	8.75	6.57	7.72	21.62	0.87	5.32	8.01	2.06	0.95	42.71	6.13	12.34
KS_E3H	6.95	8.62	6.07	7.42	24.86	0.87	6.57	8.72	0.69	1.12	40.22	8.05	8.91
KS_E4H	6.06	8.12	5.54	6.73	25.46	0.54	8.01	10.89	0.69	0.95	38.90	4.68	9.90
KS_E5H	2.52	2.65	2.37	2.41	7.89	1.11	6.28	3.82	48.36	1.88	17.58	0.00	13.09
KS_E6H	7.95	11.58	7.82	10.82	24.22	0.87	4.41	6.91	1.28	1.52	44.94	5.35	10.50
KS_E7H	4.96	5.83	3.24	3.37	24.04	2.79	6.93	18.03	1.36	1.77	19.28	20.84	4.97
KS_E8H	4.30	4.81	2.92	2.90	23.75	1.82	5.87	35.01	1.16	1.60	22.66	5.65	2.48
KS_E9H	4.49	6.14	2.22	2.16	26.12	2.27	7.40	30.31	0.39	2.45	27.45	0.00	3.60
KS_E10H	4.85	5.84	2.51	2.37	25.53	1.09	5.37	19.92	2.67	3.21	30.07	11.12	1.01
KS_E11H	4.55	5.44	2.86	3.12	21.60	1.18	4.34	38.18	4.76	1.33	24.24	0.00	4.37
KS_E12H	4.50	5.32	3.48	3.90	20.55	1.17	5.04	36.56	2.03	0.88	23.36	7.54	2.86

COMPUTATION OF THE EFFECTIVE CLAY ELASTIC TENSOR

Previous work

Perhaps the best account of how the characterization of clay elastic properties is traditionally conducted is given by Katahara (1996). Two main approaches exist, each with their respective merits and drawbacks.

The first approach consists of building on elastic data acquired on single crystals, although such data are very scarce for clay minerals. Concerning illite, there are no single-crystal data in a strict sense, but it is commonly assumed for structural and compositional reasons that illite properties should be close to those of muscovite (Tosaya, 1982). Thus, muscovite data are frequently used in place of illite. Two studies report full stiffness tensor values for muscovite with very similar results: Alexandrov and Ryzhova (1961) and Vaughan and Guggenheim (1986). As far as chlorite is concerned, two incomplete data sets on clinochlore (a magnesian chlorite) are provided by Alexandrov and Ryzhova (1961). As detailed in his paper, Katahara (1996) solves for the missing elastic modulus C_{13} in clinochlore using a velocity-density trend from other micas and assuming a

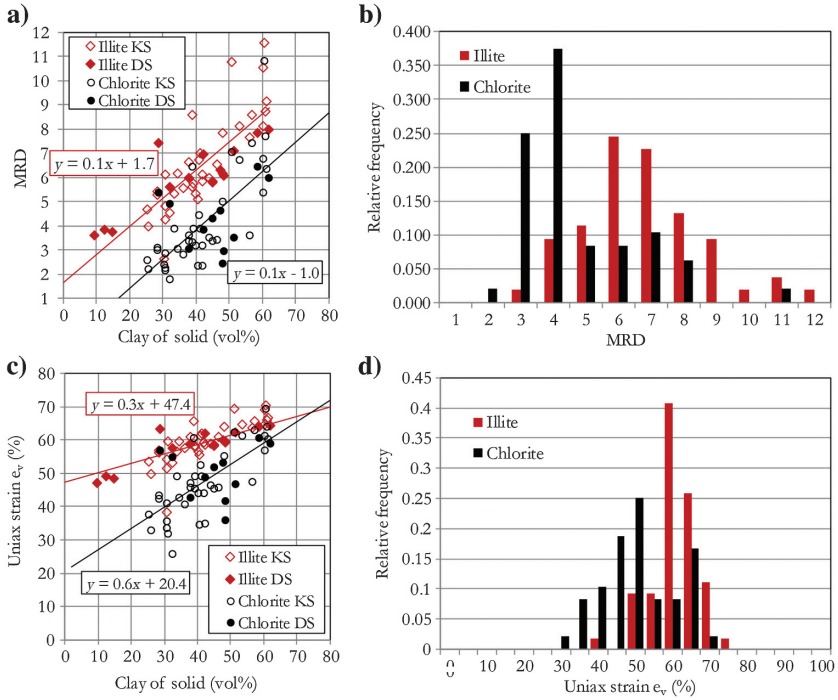

Figure 6. Summary of preferred orientation data for the two shales studied. KS, Kimmeridge Shale; DS, Devonian Shale. (a) Effect of clay abundance on MRD. (b) Distribution of MRD values in all samples for illite and chlorite. (c) Effect of clay abundance on apparent uniaxial strain (d) Distribution of apparent strain values in all samples for illite and chlorite.

Table 2. XTG and XRD data for all Devonian Shale samples studied. DS is used for Devonian Shale in the sample ID. All samples are from the same well. MRD values from UM and modified workflows are shown for comparison. XRD results are provided in vol% using equation 1.

	MRD illite (UM)	MRD illite (Shell)	MRD chlorite (UM)	MRD chlorite (Shell)	Quartz	K-feldspar	Plagioclase	Calcite	Dolomite	Pyrite	Illite	Di-oct 2:1 clays	Chlorite
ID	XTG				XRD % solid volume								
DS_1	4.54	5.63	4.06	4.93	19.2	1.2	2.7	42.6	1.4	0.5	23.3	3.5	5.6
DS_2	4.68	7.45	3.86	5.41	16.3	0.6	2.8	48.3	2.6	0.7	21.9	0.0	6.8
DS_3	6.33	7.85	5.35	6.45	23.7	0.8	4.1	7.9	2.3	2.7	34.1	16.3	8.2
DS_4	4.76	6.33	3.8	4.62	23.5	0.5	3.7	18.4	4.8	1.3	30.1	10.9	6.7
DS_5	6.32	7.99	5.08	5.99	27.8	0.9	5.3	0.3	0.4	3.2	40.2	14.8	7.1
DS_6	2.01	5.81	3.97	4.34	40.6	2.1	6.4	1.7	1.5	2.8	35.2	0.0	9.8
DS_7	—	—	—	—	15.2	1.4	2.0	64.6	3.3	1.4	10.2	0.0	2.0
DS_8	5.09	5.99	2.98	3.06	19.1	1.1	3.2	31.0	6.1	1.4	23.8	11.7	2.5
DS_9	5.43	7.09	3.01	3.53	31.5	0.8	4.9	6.3	0.7	4.3	35.5	14.3	1.8
DS_10	5.15	6.98	3.01	3.85	27.3	1.0	4.7	20.9	1.3	2.5	29.9	10.7	1.7
DS_11	5.12	6.09	2.89	2.96	35.5	0.8	4.2	7.2	1.0	2.8	34.1	13.4	1.1
DS_12	5	6.17	2.56	2.44	36.2	0.8	5.0	4.2	1.5	4.0	32.8	14.2	1.4
DS_13	3.23	3.76	—	—	48.3	2.3	2.7	24.5	5.3	2.0	14.2	0.0	0.7
DS_14	2.2	3.61	—	—	30.2	1.7	1.6	52.8	2.9	1.1	8.5	0.0	1.2
DS_15	2.99	3.87	—	—	34.3	1.3	2.2	46.1	3.2	0.4	8.6	0.0	3.9
DS_16	4.85	5.22	—	—	3.6	0.4	2.4	2.5	0.8	0.9	18.0	71.4	0.0
DS_17	—	—	—	—	88.7	1.0	1.1	1.8	1.7	0.1	2.6	0.0	3.1

mineral density of 2.71 g/cm^3. For reference, kaolinite data can also be found in the study of Alexandrov and Ryzhova. It is worth mentioning that more elastic tensor values for clays can be found in the literature in the form of first-principle calculations (i.e., Sato et al., 2005; Militzer et al., 2011), which formed the base of recent studies, such as the ones of Vasin et al. (2013) and Sayers and den Boer (2016). Typically, clay single-crystal measurements and calculations yield relatively high moduli values that are comparable with other common sedimentary minerals. This approach, which we will describe as the "dry clay approach" is rigorous in the sense that it generates reference values that should not be expected to vary significantly among published sources, as is already the case for quartz, calcite, etc. It may not be directly applicable if the clay fraction considered in the modeling has to be water bearing (in which case further work is required). An example is the work of Cholach and Schmitt (2006), who compute the effective properties of a muscovite aggregate based on assumed orientation distribution functions and then compared their anisotropic characteristics with the ones published on fully constituted shales and metamorphic schists. Other reviewed studies that build on single-crystal measurements are the ones by Wenk et al. (2007) and Lonardelli et al. (2007), who use X-ray diffraction images for estimating the orientation of clay particles.

The second approach consists of retrieving clay end-member properties from extrapolation of velocity measurements on aggregates using effective medium models. The most complete work using this type of approach is that of Wang et al. (2001) on illite, although randomly oriented aggregates were used, hence yielding only isotropic values. Another notable effort is the one of Hornby (1998), who uses the results of Marion et al. (1992) on a 20% porosity "pure shale" to retrieve a clay value at 0% porosity. This result was eventually reincorporated into an effective medium model using clay-orientation information from a thin section to compare with the Cretaceous shale measurements of Jones and Wang (1981). Sayers (2005) inverts for individual "domains" (water-clay composites) properties using assumed orientation distribution functions in the Greenhorn Shale. Bayuk et al. (2007) invert the same Greenhorn Shale data set using a different model. Finally, several popular extrapolation-based studies, i.e., considering end members such as porous/nonporous or sand/shale, were conducted by Tosaya (1982) and Han et al. (1986) using laboratory measurements and by Castagna et al. (1985) and Eastwood and Castagna (1986) using well-log data. Except for the work of Wang et al. (2001), the elastic moduli obtained for clay from inversion or extrapolation are much lower in magnitude than the ones reported for single crystals. This second approach using inversion and extrapolation provides values that in most cases incorporate an unknown amount of water. Those can prove useful in practical applications, however, especially when working with lithologic end members as opposed to mineralogical end members.

The approach followed in this paper is the one based on single-crystal measurements because no constraint exists on the quantity of adsorbed water and given the fact that very little smectite is present in the studied samples. The effective clay properties are going to be derived from XTG data using the stiffness moduli provided by Katahara (1996), which came from Alexandrov and Ryzhova (1961) (more specifically, muscovite and clinochlore for illite and chlorite, respectively). This initial set of results will be representative of a perfectly dry clay aggregate, which is consistent with a "total porosity" approach. In this case, no distinction is made between structural, adsorbed, and capillary/movable fluids and the effect of the total saturated pore space must be addressed separately. However, to provide a more versatile set of elastic moduli for the clay fraction, we will also consider the case of a "wet clay" (clay with adsorbed water) and two ways of introducing water into the aggregate will be tested so that its elastic moduli will depend not only on the direction of propagation but also on the amount of volume fraction of water.

Workflow

Anisotropic (direct) case

The procedure that is used for calculating an effective clay tensor based on orientation data is partially borrowed from Hornby et al. (1994), although that study considered fluid-clay composites as building blocks (ellipsoidal water-filled inclusions embedded in an isotropic clay background). First, clusters or bundles of particles with transverse isotropy (VTI) must be generated for each inclination angle. According to Hornby et al. (1994), it is sufficient to realize six rotations around the vertical symmetry axis to obtain such a VTI medium for a given inclination (Figure 7). These nontrivial rotations of fourth-rank tensors are executed using the Bond matrix (Mavko et al., 1998).

The orientation data obtained from XTG are then redistributed in 7.5° bins (13 bins in total from 0° to 90°), and a VTI cluster is obtained for each bin. The frequencies are scaled so that the bin at 90° angle has a frequency of one. Note that this normalization step is not strictly needed, but it offers an alternate way of comparing between different samples. Finally, all the clusters are combined according to the weights given by the chart to produce an effective clay elastic tensor.

The transversely isotropic elastic tensors for illite and chlorite taken from Katahara (1996) are as follows (values in GPa):

$$\text{Illite}: C_{ij} = \begin{bmatrix} 179.9 & 39.9 & 14.5 & 0 & 0 & 0 \\ 39.9 & 179.9 & 14.5 & 0 & 0 & 0 \\ 14.5 & 14.5 & 55 & 0 & 0 & 0 \\ 0 & 0 & 0 & 11.7 & 0 & 0 \\ 0 & 0 & 0 & 0 & 11.7 & 0 \\ 0 & 0 & 0 & 0 & 0 & 70 \end{bmatrix},$$

$$\text{Chlorite}: C_{ij} = \begin{bmatrix} 181.6 & 16.8 & 20.3 & 0 & 0 & 0 \\ 16.8 & 181.6 & 20.3 & 0 & 0 & 0 \\ 20.3 & 20.3 & 106.8 & 0 & 0 & 0 \\ 0 & 0 & 0 & 11.4 & 0 & 0 \\ 0 & 0 & 0 & 0 & 11.4 & 0 \\ 0 & 0 & 0 & 0 & 0 & 82.4 \end{bmatrix}. \quad (9)$$

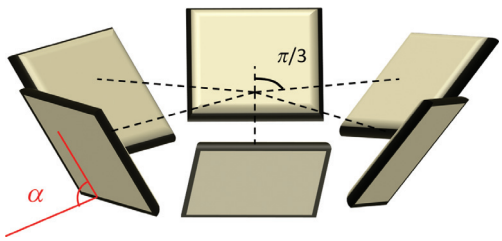

Figure 7. Representation of a set of six particles forming an elementary VTI cluster at inclination angle α.

The VTI clusters can then be combined into three effective clay tensors using, respectively, an arithmetic (or Voigt), a harmonic (or Reuss), and a geometric mean. For a given modulus C and single clay type with corresponding orientation distribution, the various averages are

$$\text{Arithmetic}: C_{\text{eff}} = \frac{1}{N}\frac{1}{6}\sum_{n=1}^{N}\sum_{i=1}^{6} D_n C_{n,i}, \tag{10}$$

$$\text{Harmonic}: \frac{1}{C_{\text{eff}}} = \frac{1}{N}\frac{1}{6}\sum_{n=1}^{N}\sum_{i=1}^{6} D_n \frac{1}{C_{n,i}}, \tag{11}$$

$$\text{Geometric}: \ln(C_{\text{eff}}) = \frac{1}{N}\frac{1}{6}\sum_{n=1}^{N}\sum_{i=1}^{6} D_n \ln(C_{n,i}), \tag{12}$$

where the subscript n, i identifies the ith particle (Figure 7) in the nth cluster with D_n being the height of the nth bin and N is the cumulative frequency in the bar chart of Figure 6b. These calculations are typically conducted separately for illite and chlorite then combined using the relative volumetric percentages obtained from the XRD data.

As a means of comparison, it is useful to compute the values of an isotropic elastic tensor for randomly oriented particles. Computing the effective properties of an aggregate of randomly oriented anisotropic particles can be achieved using existing software toolboxes such as the MTEX open-source package (Mainprice et al., 2011). However, if one seeks to determine the smallest number of particles necessary to generate an exact isotropic aggregate, the problem is not trivial. These sets of orientations have been studied for initially cubic crystal properties by Bertram et al. (2000), Noble and Man (2000), and Böhlke and Bertram (2001). Several solutions exist, some requiring a combination of only four grains to achieve isotropy. We adopted that latter approach here and proceeded with first obtaining a cubic tensor by combining three mutually perpendicular elemental VTI tensors, then using one of the four grains schemes proposed in the cited papers.

Figure 8 provides a summary of the procedure with the associated elastic tensor in the case in which a Voigt (i.e., arithmetic) average is used. In the cubic case (Figure 8b), although the stiffness is the same within all three principal planes, values obtained for instance along the [111] direction are very different. The isotropic calculation addresses this discrepancy between "in-reference" and "off-reference" stiffness values. It can be seen from Figure 8c that only one cube orientation is actually needed, the others being obtained by changing the sign of all x-coordinates, then all y-coordinates, and then all x- and y-coordinates. Therefore, only one rotation tensor has to be known, too. We provide below the rotation tensor corresponding to the blue dots in Figure 8c, which relates the coordinates of vectors in the initial reference (unprimed coordinates) to the ones of the same vectors in the rotated reference (primed coordinates):

$$\begin{pmatrix} x \\ y \\ z \end{pmatrix} = \begin{pmatrix} -0.867 & 0.413 & 0.280 \\ 0.280 & 0.867 & -0.413 \\ 0.413 & 0.280 & 0.867 \end{pmatrix} \begin{pmatrix} x' \\ y' \\ z' \end{pmatrix}. \tag{13}$$

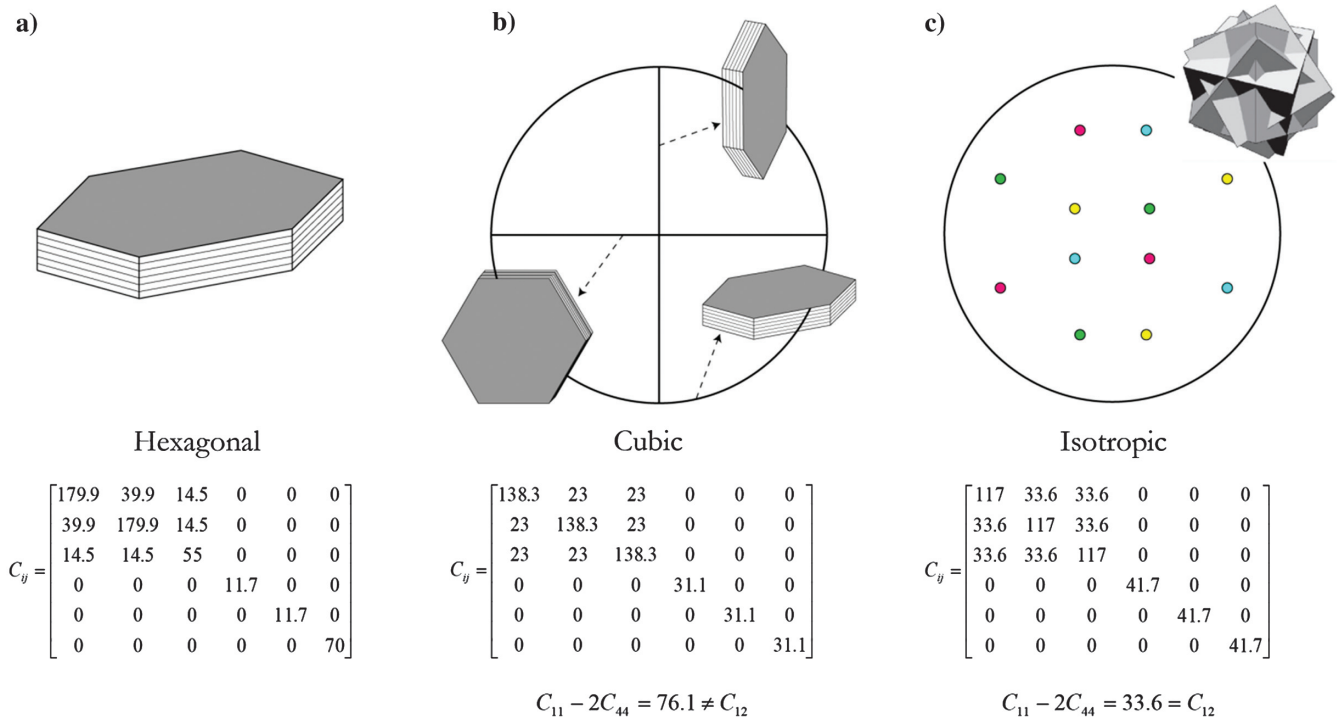

Figure 8. Derivation of an isotropic elastic tensor from an elementary VTI grain with corresponding moduli (Voigt average used in this example). (a) Initial single VTI particle (illite). (b) Cubic tensor obtained from three mutually perpendicular particles. Isotropy condition is not satisfied. (c) Isotropic tensor obtained from four cubic particles (such as in [b]). The dots represent the projections of the normals to the cube faces. A different color is used for each particle. The inset is a representation of one of the "four-grain" solutions, after Böhlke and Bertram (2001).

Apparent (or pseudo) isotropic case

The apparent or pseudoisotropic case refers to the calculation of isotropic $*K$ and $*\mu$ moduli based on single-direction measurements in an arbitrary medium, i.e., regardless of its symmetry. It is in practice what is often done in log data modeling because the full properties of the medium are not known and isotropic models are used for simplicity. The approach proposed here consists of honoring the medium anisotropy while still using isotropic models by computing isotropic moduli that vary with propagation angle. Concretely, the computation is done as follows.

Let us consider an arbitrary medium in which one P-wave and two orthogonally polarized S-waves are propagated in a given direction, the corresponding elastic moduli being respectively referred to as M, Gh, and Gv.

If the two S-wave moduli are identical (this is a particular case, e.g., vertical propagation in a VTI medium), then $*K$ and $*\mu$ are written

$$\mu^* = G_h = G_v \quad \text{and} \quad K^* = M - \frac{4}{3} \times \mu^*. \tag{14}$$

If the two S-wave velocities are different, the bulk modulus can be calculated using the average of the two shear moduli:

$$\mu^* = \frac{1}{2} \times (G_h + G_v) \quad \text{and}$$
$$K^* = M - \frac{4}{3} \times \mu^*. \tag{15}$$

Alternatively, it is possible to consider only one S-wave modulus and bypass the averaging done above. In the discussion, the approximation made in equation 14 will be briefly discussed.

The important aspect here is that, based on a table derived from the computation of apparent isotropic moduli, one should be able to pick an appropriate set of bulk and shear moduli when using an isotropic effective medium model given a known angle of propagation with respect to the VTI reference.

Results

In Figure 9, the result of the elastic moduli calculation in the 36 Kimmeridgian Shale (Figure 9a) and 11 Devonian Shale (Figure 9b) samples is shown for the case in which the geometric mean is used. Values obtained for the isotropic case are added for comparison. Individual samples are not identified, but it is clear that the range of variability for each individual modulus is very limited, except for two Kimmeridgian Shale samples in which the measured chlorite content is significantly higher, the effect of which is best seen on C_{33} (compressive stiffness along the vertical symmetry axis). The variability associated with the choice of averaging method was comparable with that observed among samples. Note that the large contrasts that were observed in the MRD values from XTG do not translate into large changes in elastic properties. This point is discussed in detail in the next section.

DISCUSSION

We carry out here the comparison between orientation data and resulting effective elastic properties. More specifically, this comparison aims to answer the following questions:

- What effective clay elastic anisotropy is to be expected from the particle preferred orientation?
- What are the respective contributions of a change in clay content versus a change in the intensity of the preferred orientation (MRD)? In other words, do we need XTG data as much as we need clay content information?
- What clay elastic moduli should be used in effective medium models to reflect its anisotropic contribution?
- In lithology-based modeling, what numbers should be used for effective "wet" clay properties?

Effect of preferred orientation on the clay elastic tensor

The direct effect of MRD on individual effective elastic moduli and associated anisotropy is evaluated here. Figure 10a shows the

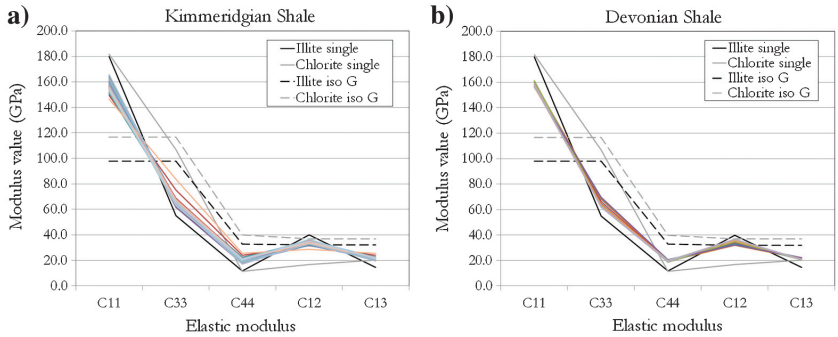

Figure 9. Result of effective dry clay elastic tensor calculation using the geometric mean. (a) Elastic constants of the effective clay VTI medium for 36 Kimmeridgian Shale samples (colored lines). (b) Elastic constants of the effective clay VTI medium for 11 Devonian Shale samples (colored lines).

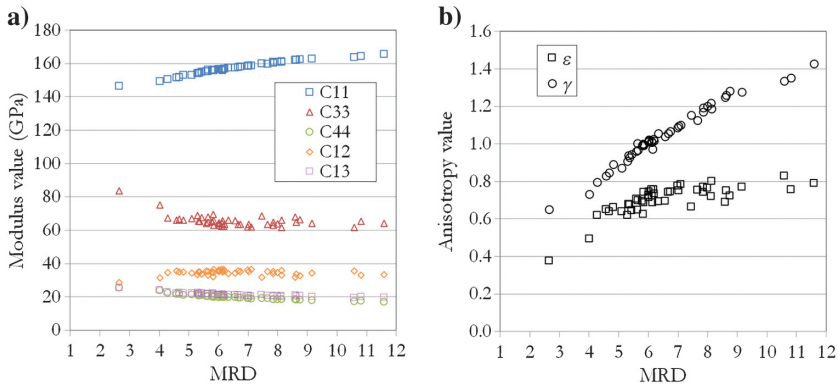

Figure 10. (a) Individual effective elastic moduli as a function of the MRD value for illite in all Kimmeridgian Shale samples. (b) Associated Thomsen's anisotropy parameters ε and γ for P- and S-waves.

moduli values calculated for all Kimmeridgian Shale samples as a function of MRD value then the associated Thomsen compressional (P) and shear (S) anisotropy parameters ε and γ, which are defined as follows (Thomsen, 1986):

$$\varepsilon = \frac{C_{11} - C_{33}}{2C_{33}}; \quad \gamma = \frac{C_{66} - C_{44}}{2C_{44}}. \tag{16}$$

As far as individual moduli are concerned, changes associated with MRD are fairly small compared with the MRD values themselves. Although MRD values vary at least threefold, elastic moduli typically vary by approximately 10%. This is due to the fact that the individual particle orientations are averaged out in the effective property calculation. Thomsen's anisotropy parameters show more sensitivity to the MRD (Figure 10b). Most of the P-wave modulus anisotropy data are comprised between 0.6 and 0.8, and in the case of S-wave modulus anisotropy, that range is approximately 0.8–1.3. These translate respectively into actual velocity ratios ranges of $V_{P_{min}}/V_{P_{max}} = 0.62 - 0.67$ and $V_{S_{min}}/V_{S_{max}} = 0.53 - 0.62$. Although these ratios are low, reflecting a very high degree of anisotropy, their respective ranges are actually moderate. Note also that the MRD range covered by this data set is very large; therefore, this result should be generally applicable for clay in shale rock.

Change in preferential orientation versus change in clay content

The effect of clay on the effective rock properties is not only controlled by clay intrinsic properties and orientation, but also by the clay fraction. Comparing the effects of preferential orientation and clay fraction can help to assess how important it is to precisely know the clay preferential orientation in a given sample. The conceptual difference between the two effects is illustrated in Figure 11. To test for this effect, we create an imaginary solid aggregate of clay, quartz, and calcite, in which only the clay exhibits intrinsic anisotropic properties, and where quartz and calcite are present in equal proportions. A geometric average is used among the components of the elastic tensor. Then, we consider two cases. In case 1, we directly use s sample-wise result for the clay effective properties, i.e., taking into account the orientation data and the clay content (vol% of solid fraction calculated from Table 2). In case 2, we first calculate an average clay tensor from all the results obtained in Figure 9 and then we proceed as in case (1) using this average clay tensor and clay content for all samples.

The results of the test for the Kimmeridgian Shale samples are showed in Figure 12 for the individual moduli and Thomsen's anisotropy parameters. All the variables are plotted against the clay fraction of the solid.

In Figure 12a, it is clear that cases 1 and 2 differ very little in terms of the stiffness values. Some drift exists from one data set to the other due to the effect of clay content on preferential orientation (as was shown in Figure 6), but for the effective medium, it actually results in a minimal deviation. A very similar observation can be made for Thomsen's anisotropy parameters in Figure 12b. The colored areas represent the difference to be expected between cases 1 and 2. To illustrate the impact of the largest discrepancy, the S-wave ratio at a high clay content would be about $V_{S_{min}}/V_{S_{max}} = 0.69$ using the average clay tensor instead of $V_{S_{min}}/V_{S_{max}} = 0.66$ if the sample-wise XTG results are used. Such differences are very minor, which provides us with the important conclusion that because changes in clay content have a much greater impact on the anisotropy of the effective medium than fluctuations in clay preferred orientation, it is reasonable to propose the use of a single clay elastic tensor for rock-modeling applications. This should be independent of the exact clay tensor used and therefore hold true for water-saturated clay. If the tensors obtained in Kimmeridgian and Devonian Shales are combined (47 data points), this average dry clay tensor may be written as follows (values in GPa):

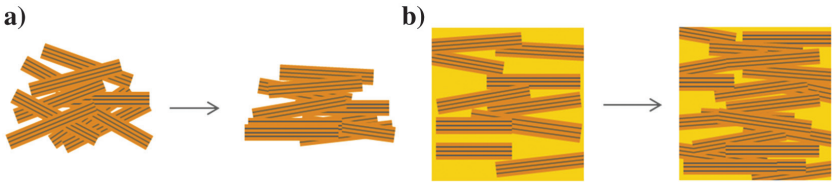

Figure 11. (a) Increase in anisotropy due to the increase in preferred orientation and (b) increase in anisotropy due to the increase in clay content.

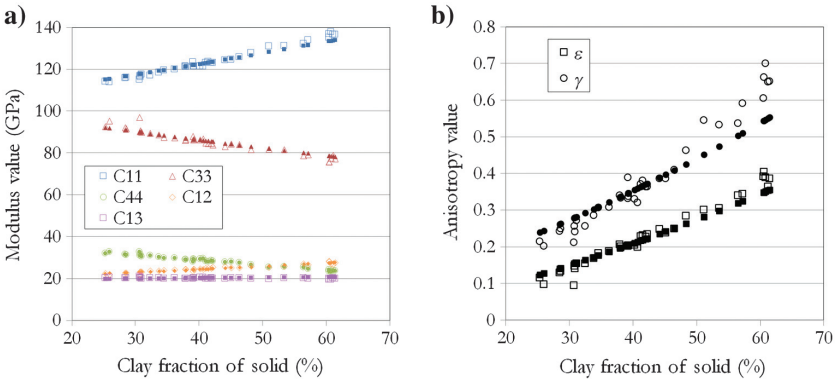

Figure 12. (a) Open symbols, elastic moduli for a clay/quartz/calcite aggregate as a function of clay fraction of solid using the clay tensors plotted in Figure 9 (case 1); solid symbols the same calculation assuming a constant average clay tensor (case 2). (b) Thomsen's anisotropy parameters ε and γ for cases (1 and 2) using the same nomenclature as in (a) for symbols.

$$C_{ij,\text{clay}} = \begin{bmatrix} 157.3 & 34.5 & 21.4 & 0 & 0 & 0 \\ 34.5 & 157.3 & 21.4 & 0 & 0 & 0 \\ 21.4 & 21.4 & 65.6 & 0 & 0 & 0 \\ 0 & 0 & 0 & 20 & 0 & 0 \\ 0 & 0 & 0 & 0 & 20 & 0 \\ 0 & 0 & 0 & 0 & 0 & 61.4 \end{bmatrix}. \tag{17}$$

The variability in the values of the effective moduli in Figure 9, which reflects the different cases of preferred orientation and illite to chlorite ratio, results in an estimated uncertainty in the moduli of the average clay tensor that ranges from approximately 5% (C_{11}) to 15% (C_{44}). It is worth noting here that the residuals that were obtained in the processing of the XTG data (Figure 5) contribute very little to that uncertainty because the vari-

ability associated with the residuals for a given sample is small compared with the variability observed within the group of samples due to differences in preferred orientation and illite to chlorite ratio. Also, the tensor in equation 16 should be considered valid for illite-dominated clay assemblages only because C_{12} and C_{33} are very different between illite and chlorite and a high relative chlorite content would cause significant changes in the effective values for these two moduli.

Pseudoisotropic elastic moduli for isotropic rock models

If one uses an isotropic approach for modeling rock elastic properties, appropriate moduli still have to be chosen. Because a random orientation of clay particles is very unlikely, one might conclude that isotropic moduli are inappropriate. An example of a consequence of this for propagation perpendicular to bedding (e.g., in the case of a vertical well) is the need to soften the matrix by adding microcracks because the clay stiffness was initially overestimated. Conversely, one could expect the use of isotropic moduli to lead to an underestimation of porosity for propagation along the bedding plane. We propose here to introduce directionally dependent isotropic moduli $*K$ and $*\mu$, which we call apparent or pseudoisotropic moduli.

In Figure 13, changes in $*K$ and $*\mu$ are plotted in polar coordinates and compared with the reference isotropic moduli. Figure 13a first shows for reference the profile of moduli values M, Gh and Gv obtained directly from the clay tensor in equation 16 and which would be used to compute the phase velocities V_P, V_{SH}, and V_{SV}. In Figure 13b, the two pseudoisotropic moduli are plotted as a function of propagation angle and compared with reference isotropic values from Mavko et al. (1998) (muscovite, three sets of values), Wang et al. (2001), and from this work using the isotropic calculation illustrated in Figure 8 and a geometric average. In the case of vertical propagation, pseudoisotropic bulk and shear moduli are lower than all their isotropic counter parts, suggesting a substantial chance of overestimating the clay stiffness when using usual isotropic values. As the angle increases toward 90° (along bedding propagation), the pseudoisotropic shear modulus matches the higher isotropic estimate, whereas the pseudoisotropic bulk modulus is nearly twice the reference isotropic values. These observations suggest that the concept of angle-dependent isotropic moduli can greatly improve the way the effect of clay is accounted for in rock models. Note that in the approach followed here, simplicity is achieved at the cost of making a substantial approximation on the S-wave modulus, especially in the case of propagation parallel to the symmetry plane in which the two initial perpendicularly polarized S-waves are the most different. Depending on the situation at hand, if two very distinct S-wave velocities are available from e.g., well logs, then, two pseudoisotropic media may be considered, which would each have a different pair of bulk and shear moduli. Although this approach is more rigorous, it would also take away from the simplicity of the concept and, if shear splitting is observed, one would have to be certain that it is caused by clay or by a feature that shares the same symmetry and principal axes.

Effect of water content on clay tensor and pseudoisotropic moduli

So far, all of the elastic calculations have used dry clay. We propose in this section to put forth two strategies for incorporating water into the effective clay aggregate. Note that because inclusion models are used, we will use the term porosity here, although that is meant to constitute the water fraction bound to the clay aggregate and not the actual porosity of the shale sample. The first strategy,

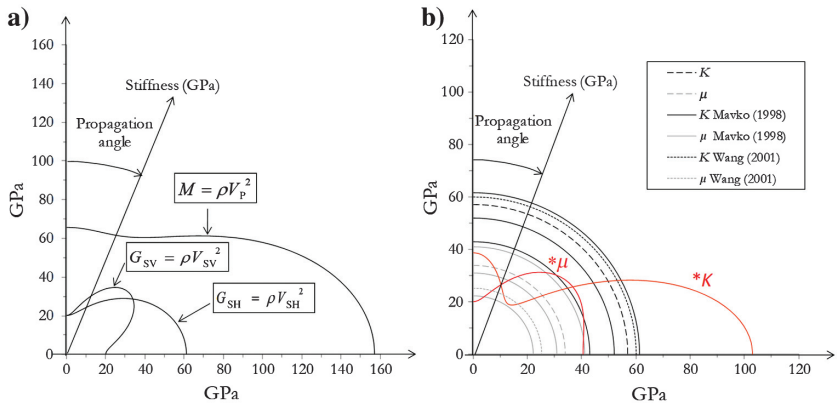

Figure 13. (a) Polar representation for the wave modulus M and two shear moduli Gh and Gv from the average clay tensor in equation 17. (b) Corresponding pseudoisotropic bulk and shear moduli (in red), where the shear modulus is obtained as the average of the two shear moduli in (a). Background quarter circles represent reference isotropic values from Mavko et al. (1998) (three values, solid lines) and Wang et al. (2001) (short dashes). The lines with long dashes are the isotropic values calculated in this work.

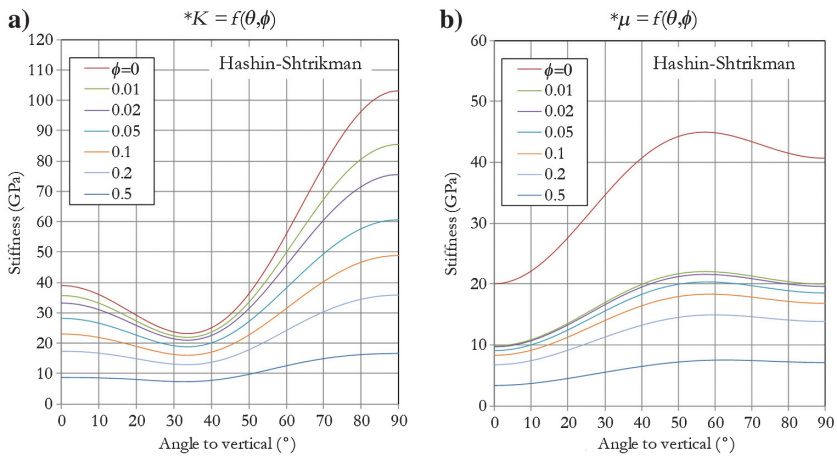

Figure 14. (a) Evolution of the apparent bulk modulus $*K$ as a function of angle to the vertical axis for idealized equant porosity with values up to 50% using the average of the Hashin-Shtrikman bounds. (b) Evolution of the apparent shear modulus $*\mu$ as a function of angle to the vertical axis for porosities up to 50% using the average of the Hashin-Shtrikman bounds.

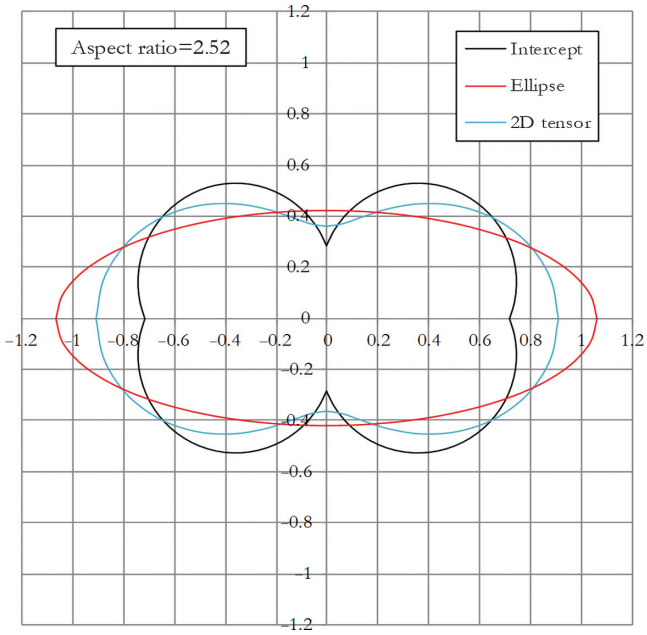

Figure 15. Effective pore shape calculated from average illite preferred orientation data in the Kimmeridgian Shale. Black, effective pore shape from intercept data assuming a population of flat pores; red, pore shape of identical aspect ratio and surface used in the ellipsoidal inclusion model (actual ellipse); blue, pore shape of identical aspect ratio and surface assuming an elliptical function of the form $f(\theta) = A\cos^2(\theta) + B\sin^2(\theta)$ (elliptical anisotropy).

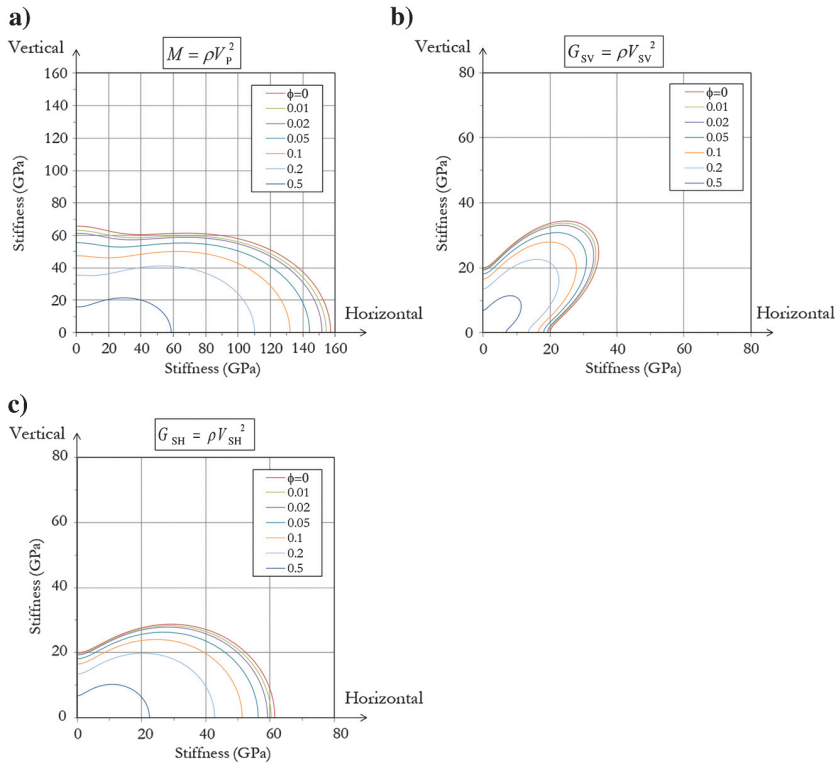

Figure 16. Effective elastic moduli obtained for the average clay tensor as a function of propagation angle with varying amounts of water-filled porosity. (a) P-wave modulus, (b) vertical S-wave modulus, and (c) horizontal S-wave modulus.

which is the simplest, consists of directly calculating the Hashin-Shtrikman bounds of a clay/water mixture starting from the pseudoisotropic moduli of Figure 13b. Such a calculation implies that the porosity is equant, which is not rigorously true. But this method is tried as a first approximation and is an easily applicable approach. The second strategy consists of using a recent derivation that provides the effective properties of a medium composed of anisotropic inclusions embedded in an anisotropic background (Sevostianov et al., 2005).

The result of the first approach using the Hashin-Shtrikman bounds (for corresponding equations, see, e.g., Mavko et al., 1998) is provided in Figure 14 for $*K$ and $*\mu$ with porosities varying roughly on a log scale from 1% to 50%. As expected, regardless of the porosity, values calculated horizontally are systematically larger than the ones calculated vertically, but the anisotropy is noticeably reduced by the incorporation of an increasing fraction of equant porosity.

For the second approach, in which the effective clay tensor in equation 16 is used, one needs to define the anisotropy of the pore space to enter the calculation. This is done by assuming that the porosity presents the same preferred orientation as the host clay material because adsorbed water is expected to be incorporated in conformance with the grain geometry. Computing the average particle distribution for all illite measurements in Kimmeridgian Shale provides an average distribution of flat pores. This distribution can then be used to estimate the pore-shape anisotropy by calculating the aspect ratio of the corresponding orientation tensor. This is done by calculating the intercept value (the sum of projection of all flat objects perpendicularly to the direction of observation; Underwood, 1970) in two dimensions.

Figure 15 illustrates the result obtained from the intercept and provides the result of the pore-shape aspect ratio calculation to be used in the computation (the pore-aspect ratio = 2.52). Note that the effective pore shape that is obtained (in black) differs quite substantially from the one of the ellipse (in red), which is the one used in the inclusion model of Sevostianov et al. (2005). The blue curve, which is not used in any computation here, is an attempt to model the shape of the intercept profile using an elliptical function of the form $f(\theta) = A\cos^2(\theta) + B\sin^2(\theta)$, keeping the aspect ratio and surface the same as for the other shapes. An even better fit could be obtained by introducing the equivalent of Thomsen's (1986) δ parameter.

Using a pore-aspect ratio of 2.52 and water properties for the inclusion elastic tensor ($K = 2.2$ GPa; $\mu = 0$ GPa), the Sevostianov model is applied to the effective clay elastic tensor for the same porosity range as was used with the Hashin-Shtrikman approach. First, we show the results for the three moduli (P-wave modulus, vertical shear modulus, and horizontal shear modulus) as a function of angle (deviation from the vertical) and porosity in Figure 16. Note the relative stability of the anisotropy for the P-wave and horizontal S-wave moduli up to an angle of approximately 60° from the vertical direction.

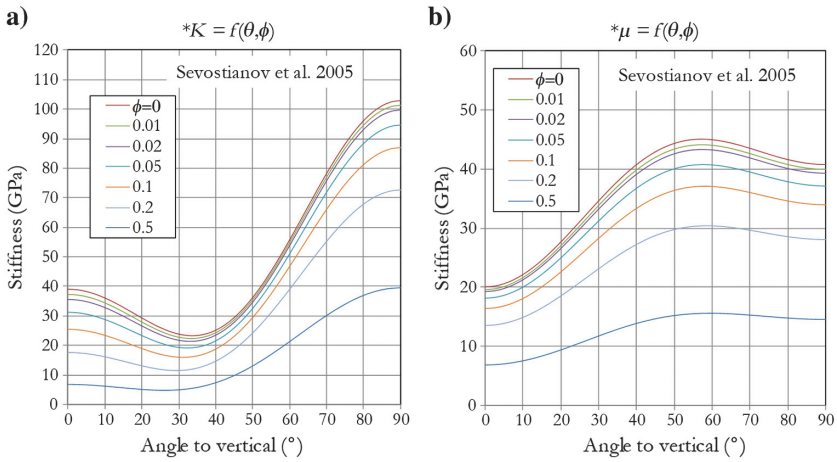

Figure 17. Apparent isotropic elastic moduli calculated using Sevostianov et al. (2005) approach as a function of angle for porosities up to 50%. (a) Apparent bulk modulus $*K$ and (b) apparent shear modulus $*\mu$.

Next, in Figure 17, the apparent bulk and shear moduli $*K$ and $*\mu$ are calculated from the curves of Figure 16.

Comparing the Hashin-Shtrikman (HS) and Sevostianov approaches in Figures 14 and 17, two main observations can be made: (1) As far as the bulk modulus is concerned, little difference is seen in the case of vertical propagation. For horizontal propagation, the HS bulk modulus decreases faster with porosity, compared with the Sevostianov one, which is a direct effect of the pore-shape anisotropy because pores are preferentially aligned horizontally. (2) Looking at the shear modulus, the effect of the zero shear stiffness for water in the HS case yields a very different evolution as a function of porosity with a sharp initial drop from the nonporous case. This may not represent the actual effect of water here because the shear properties of adsorbed water are probably different from null and the HS approach assumes the presence of a continuous coat on harder grains in the lower bound case.

The Sevostianov approach likely constitutes a better approximation of the elastic behavior of an actual aggregate. In general, the properties reported for various effective clays in the literature are well-represented by the ranges calculated for subvertical propagation. The changes that occur at a higher angle, however, directly reflect clay anisotropy and should be used when modeling the properties along deviated/horizontal well trajectories. We believe that the apparent or pseudoisotropic moduli approach offers a state-of-the-art physical ground and very straightforward applicability. For more accurate results, the full calculation comprising three elastic moduli as a function of angle, as illustrated in Figure 16, should be used.

CONCLUSION

In this study, XRD and XTG data were used to quantify the effect of clay content and preferred orientation on elastic anisotropy in two well-known North American gas-shale formations. Based on the computations conducted, it was found that the clay content has a major impact on the overall anisotropy and that changes in the clay preferred orientation are of lesser importance. As a result, this work suggests that the use of a single clay elastic tensor to represent the clay contribution to effective rock properties can be a sufficient approximation. Then, we modified this tensor to incorporate the influence of water content using two different homogenization schemes for a large range of water-fraction values. To further facilitate the use of these calculations, we also introduced the concept of apparent or pseudoisotropic bulk and shear moduli, allowing one to modify how clay should contribute to the effective medium properties given a propagation angle even when isotropic models are used.

Overall, our study demonstrates that, even for normal-to-bedding propagation, the clay anisotropy should be accounted for, and we provide a tool to reflect this contribution whether isotropic or anisotropic models are used.

This derivation also enables us to progress further toward isolating the contribution of a structural component in the effective rock properties after the removal of additional isotropic mineral contributions, provided that the total porosity can be estimated with reasonable accuracy.

ACKNOWLEDGMENTS

HRXTG is supported by the Electron Microbeam Analysis Laboratory at the UM and NSF grant EAR-0345985, and we thank B. A. van der Pluijm for access to HRXTG. Shell International E&P Inc. is thanked for permission to publish and for financial support. We are also indebted to all the reviewers who provided insightful comments and subject matter knowledge that significantly improved this paper.

REFERENCES

Alexandrov, K. S., and T. V. Ryzhova, 1961, Elastic properties of rock forming minerals 2: Layered silicates: Bulletin USSR Academy of Science, Geophysics Series, **11**, 871–875.

Allan, A. M., W. Kanitpanyacharoen, and T. Vanorio, 2015, A multiscale methodology for the analysis of velocity anisotropy in organic-rich shale: Geophysics, **80**, no. 4, C73–C88, doi: 10.1190/geo2014-0192.1.

Baker, D. W., K. S. Chawla, and R. J. Krizek, 1993, Compaction fabrics of pelites: Experimental consolidation of kaolinite and implications for analysis of strain in slate: Journal of Structural Geology, **15**, 1123–1137, doi: 10.1016/0191-8141(93)90159-8.

Banik, N. C., 1984, Velocity anisotropy of shales and depth estimation in the North-Sea Basin: Geophysics, **49**, 1411–1419, doi: 10.1190/1.1441770.

Bayuk, I. O., M. Ammerman, and E. M. Chesnokov, 2007, Elastic moduli of anisotropic clay: Geophysics, **72**, no. 5, D107–D117, doi: 10.1190/1.2757624.

Bertram, A., T. Böhlke, N. Gaffke, B. Heiligers, and R. Offinger, 2000, On the generation of discrete isotropic orientation distributions for linear elastic cubic crystals: Journal of Elasticity and the Physical Science of Solids, **58**, 233–248, doi: 10.1023/A:1007655817328.

Böhlke, T., and A. Bertram, 2001, Isotropic orientation distributions of cubic crystals: Journal of the Mechanics and Physics of Solids, **49**, 2459–2470, doi: 10.1016/S0022-5096(01)00063-1.

Castagna, J. P., M. L. Batzle, and R. L. Eastwood, 1985, Relationships between compressional-wave and shear-wave velocities in clastic silicate rocks: Geophysics, **50**, 571–581, doi: 10.1190/1.1441933.

Cholach, P. Y., and D. R. Schmitt, 2006, Intrinsic elasticity of a textured transversely isotropic muscovite aggregate: Comparisons to the seismic anisotropy of schists and shales: Journal of Geophysical Research, **111**, B09410, doi: 10.1029/2005JB004158.

Curtis, C. D., S. R. Lipshie, G. Oertel, and M. J. Pearson, 1980, Clay orientation in some Upper Carboniferous mudrocks, its relationship to quartz content and some inferences about fissility, porosity and compactional

history: Sedimentology, **27**, 333–339, doi: 10.1111/j.1365-3091.1980.tb01183.x.
Day-Stirrat, R. J., A. C. Aplin, J. Srodon, and B. A. van der Pluijm, 2008, Diagenetic reorientation of phyllosilicate minerals in Paleogene mudstones of the Podhale Basin, southern Poland: Clays and Clay Minerals, **56**, 100–111, doi: 10.1346/CCMN.2008.0560109.
Day-Stirrat, R. J., S. P. Dutton, K. L. Milliken, R. G. Louks, A. C. Aplin, S. Hillier, and B. A. van der Pluijm, 2010a, Fabric anisotropy induced by primary depositional variations in the silt: Clay ratio in two fine-grained slope fan complexes: Texas Gulf Coast and northern North Sea: Sedimentary Geology, **226**, 42–53, doi: 10.1016/j.sedgeo.2010.02.007.
Day-Stirrat, R. J., K. L. Milliken, S. P. Dutton, R. G. Louks, S. Hillier, A. C. Aplin, and A. M. Schleicher, 2010b, Open-system chemical behavior in deep Wilcox Group mudstones, Texas Gulf Coast, USA: Marine and Petroleum Geology, **27**, 1804–1818, doi: 10.1016/j.marpetgeo.2010.08.006.
Eastwood, R. L., and J. P. Castagna, 1986, Interpretation of V_P/V_S ratios from sonic logs, *in* S. H. Danbom and S. N. Domenico, eds., Shear-wave exploration: SEG, 139–153.
Evans, K. F., G. Oertel, and T. Engelder, 1989, Appalachian stress study: 2. Analysis of Devonian shale core: Some implications for the nature of contemporary stress variations and Alleghanian deformation in Devonian rocks: Journal of Geophysical Research, **94**, 7155–7170, doi: 10.1029/JB094iB06p07155.
Haines, S. H., B. A. van der Pluijm, M. J. Ikari, D. M. Saffer, and C. Marone, 2009, Clay fabric intensity in natural and artificial fault gouges: Implications for brittle fault zone processes and sedimentary basin clay fabric evolution: Journal of Geophysical Research-Solid Earth, **114**, B05406, doi: 10.1029/2008JB005866.
Han, D. H., A. Nur, and D. Morgan, 1986, Effects of porosity and clay content on wave velocities in sandstones: Geophysics, **51**, 2093–2107, doi: 10.1190/1.1442062.
Henry, P., L. Jouniaux, E. J. Screaton, S. Hunze, and D. M. Saffer, 2003, Anisotropy of electrical conductivity record of initial strain at the toe of the Nankai accretionary wedge: Journal of Geophysical Research, **108**, 2407, doi: 10.1029/2002JB002287.
Ho, N. C., D. R. Peacor, and B. A. van der Pluijm, 1995, Reorientation mechanisms of clay minerals in the mudstone-to-slate transition at Lehigh Gap, Pennsylvania: Journal of Structural Geology, **17**, 345–356, doi: 10.1016/0191-8141(94)00065-8.
Ho, N. C., D. R. Peacor, and B. A. van der Pluijm, 1999, Preferred orientation of clay minerals in Gulf Coast mudstones and relation to the smectite-illite transition: Clays and Clay Minerals, **47**, 495–504, doi: 10.1346/CCMN.1999.0470412.
Hornby, B. E., 1998, Experimental laboratory determination of the dynamic elastic properties of wet, drained shales: Journal of Geophysical Research-Solid Earth, **103**, 29945–29964, doi: 10.1029/97JB02380.
Hornby, B. E., L. M. Schwartz, and J. A. Hudson, 1994, Anisotropic effective-medium modeling of the elastic properties of shales: Geophysics, **59**, 1570–1583, doi: 10.1190/1.1443546.
Jacob, G., H. J. Kisch, and B. A. van der Pluijm, 2000, The relationship of phyllosilicate orientation, X-ray diffraction intensity ratios, and c/b fissility ratios in metasedimentary rocks of the Helvetic zone of the Swiss Alps and the Caledonides of Jamtland, central western Sweden: Journal of Structural Geology, **22**, 245–258, doi: 10.1016/S0191-8141(99)00149-2.
Johansen, T. A., B. O. Ruud, and M. Jakobsen, 2004, Effect of grain scale alignment on seismic anisotropy and reflectivity of shales: Geophysical Prospecting, **52**, 133–149, doi: 10.1046/j.1365-2478.2003.00405.x.
Johnston, J. E., and N. I. Christensen, 1995, Seismic anisotropy of shales: Journal of Geophysical Research-Solid Earth, **100**, 5991–6003, doi: 10.1029/95JB00031.
Jones, L. E. A., and H. F. Wang, 1981, Ultrasonic velocities in Cretaceous shales from the Williston Basin: Geophysics, **46**, 288–297, doi: 10.1190/1.1441199.
Kanitpanyacharoen, W., F. B. Kets, H.-R. Wenk, and R. Wirth, 2012, Mineral preferred orientation and microstructure in the Posidonia Shale in relation to different degrees of thermal maturity: Clays and Clay Minerals, **60**, 315–329, doi: 10.1346/CCMN.2012.0600308.
Katahara, K., 1996, Clay mineral elastic properties: 66th Annual International Meeting, SEG, Expanded Abstracts, 1691–1694, doi: 10.1190/1.1826454.
Lonardelli, I., H. Wenk, and Y. Ren, 2007, Preferred orientation and elastic anisotropy in shales: Geophysics, **72**, no. 2, D33–D40, doi: 10.1190/1.2435966.
Mainprice, D., R. Hielscher, and H. Schaeben, 2011, Calculating anisotropic physical properties from texture data using the MTEX open source package, *in* D. J. Prior, E. H. Rutter, and D. J. Tatham, eds., Deformation mechanisms, rheology and tectonics: Microstructures, mechanics and anisotropy: Geological Society, Special Publications 360, 175–192.
March, A., 1932, Mathematical theory on regulation according to the particle shape in affine deformation: Zeitschrift fur Kristallographie, **81**, 285.
Marion, D., A. Nur, H. Yin, and D. Han, 1992, Compressional velocity and porosity in sand-clay mixtures: Geophysics, **57**, 554–563, doi: 10.1190/1.1443269.
Mavko, G., T. Mukerji, and J. Dvorkin, 1998, The rock physics handbook: Tools for seismic analysis in porous media: Cambridge University Press, 329.
Militzer, B., H. Wenk, S. Stackhouse, and L. Stixrude, 2011, First-principles calculation of the elastic moduli of sheet silicates and their application to shale anisotropy: American Mineralogist, **96**, 125–137, doi: 10.2138/am.2011.3558.
Moyano, B., K. Spikes, T. A. Johansen, and N. H. Mondol, 2012, Modeling compaction effects on the elastic properties of clay-water composites: Geophysics, **77**, no. 5, D171–D183, doi: 10.1190/geo2011-0426.1.
Noble, L., and C. S. Man, 2000, Designing textured polycrystals with specific isotropic material tensor: The ODF method: Rendiconti del Seminario Matematico, **58**, 155–170.
Oertel, G., 1983, The relationship of strain and preferred orientation of phyllosilicate grains in rocks: A review: Tectonophysics, **100**, 413–447, doi: 10.1016/0040-1951(83)90197-X.
Owens, W. H., 1973, Strain modification of angular density distributions: Tectonophysics, **16**, 249–261, doi: 10.1016/0040-1951(73)90014-0.
Rundle, J. B., and K. W. Schuler, 1981, A composite model for the anisotropic elastic moduli of lean oil shale: Geophysics, **46**, 163–171, doi: 10.1190/1.1441186.
Sato, H., K. Ono, C. T. Johnston, and A. Yamagishi, 2005, First-principles studies on the elastic constants of a 1:1 layered kaolinite mineral: American Mineralogist, **90**, 1824–1826, doi: 10.2138/am.2005.1832.
Sayers, C. M., 1994, The elastic anisotropy of shales: Journal of Geophysical Research-Solid Earth, **99**, 767–774, doi: 10.1029/93JB02579.
Sayers, C. M., 1999, Stress-dependent seismic anisotropy of shales: Geophysics, **64**, 93–98, doi: 10.1190/1.1444535.
Sayers, C. M., 2005, Seismic anisotropy of shales: Geophysical Prospecting, **53**, 667–676, doi: 10.1111/j.1365-2478.2005.00495.x.
Sayers, C. M., 2008, The effect of low aspect ratio pores on the seismic anisotropy of shales: 78th Annual International Meeting, SEG, Expanded Abstracts, 2750–2754, doi: 10.1190/1.3063916.
Sayers, C. M., 2013, The effect of kerogen on the elastic anisotropy of organic-rich shales: Geophysics, **78**, no. 2, D65–D74, doi: 10.1190/geo2012-0309.1.
Sayers, C. M., and L. D. den Boer, 2016, The elastic anisotropy of clay minerals: Geophysics, **81**, no. 5, C193–C203, doi: 10.1190/geo2016-0005.1.
Sevostianov, I., N. Yilmaz, V. Kushch, and V. Levin, 2005, Effective elastic properties of matrix composites with transversely-isotropic phases: International Journal of Solids and Structures, **42**, 455–476, doi: 10.1016/j.ijsolstr.2004.06.047.
Sintubin, M., 1994, Phyllosilicate preferred orientation in relation to strain path determination in the Lower Paleozoic Stavelot-Venn Massif (Ardennes, Belgium): Tectonophysics, **237**, 215–231, doi: 10.1016/0040-1951(94)90256-9.
Solum, J. G., and B. A. van der Pluijm, 2009, Quantification of fabrics in clay gouge from the Carboneras fault, Spain and implications for fault behavior: Tectonophysics, **475**, 554–562, doi: 10.1016/j.tecto.2009.07.006.
Solum, J. G., B. A. van der Pluijm, and D. R. Peacor, 2005, Neocrystallization, fabrics and age of clay minerals from an exposure of the Moab Fault, Utah: Journal of Structural Geology, **27**, 1563–1576, doi: 10.1016/j.jsg.2005.05.002.
Solum, J. G., B. A. van der Pluijm, D. R. Peacor, and L. N. Warr, 2003, Influence of phyllosilicate mineral assemblages, fabrics, and fluids on the behavior of the Punchbowl fault, southern California: Journal of Geophysical Research-Solid Earth, **108**, 2233, doi: 10.1029/2002JB001858.
Thomsen, L., 1986, Weak elastic anisotropy: Geophysics, **51**, 1954–1966, doi: 10.1190/1.1442051.
Tosaya, C. A., 1982, Acoustical properties of clay-bearing rocks: Ph.D. thesis, Stanford University.
Underwood, E. E., 1970, Quantitative stereology: Addison-Wesley.
van der Pluijm, B. A., N.-C. Ho, and D. R. Peacor, 1994, High-resolution X-ray texture goniometry: Journal of Structural Geology, **16**, 1029–1032, doi: 10.1016/0191-8141(94)90084-1.
Vasin, R. N., H. R. Wenk, W. Kanitpanyacharoen, S. Matthies, and R. Wirth, 2013, Elastic modeling of Kimmeridge shale: Journal of Geophysical Research, **118**, 3931–3956, doi: 10.1002/jgrb.50259.
Vaughan, M. T., and S. Guggenheim, 1986, Elasticity of muscovite and its relationship to crystal structure: Journal of Geophysical Research, **91**, 4657–4665, doi: 10.1029/JB091iB05p04657.
Vernik, L., and C. Landis, 1996, Elastic anisotropy of source rocks: Implications for hydrocarbon generation and primary migration: AAPG Bulletin, **80**, 531–544.

Vernik, L., and X. Z. Liu, 1997, Velocity anisotropy in shales: A petrophysical study: Geophysics, **62**, 521–532, doi: 10.1190/1.1444162.
Wang, Z., H. Wang, and M. E. Cates, 2001, Effective elastic properties of solid clays: Geophysics, **66**, 428–440, doi: 10.1190/1.1444934.
Wenk, H., I. Lonardelli, H. Franz, K. Nihei, and S. Nakagawa, 2007, Preferred orientation and elastic anisotropy of illite-rich shale: Geophysics, **72**, no. 2, E69–E75, doi: 10.1190/1.2432263.
Wenk, H. R., ed., 1985, Preferred orientation in deformed rocks: Academic Press.
Wenk, H.-R., M. Voltolini, M. Mazurek, L. R. Van Loon, and A. Vinsot, 2008, Preferred orientations and anisotropy in shales: Callovo-Oxfordian Shale (France) and Opalinus Clay (Switzerland): Clays and Clay Minerals, **56**, 285–306, doi: 10.1346/CCMN.2008.0560301.